ACS Biomaterials SCIENCE & ENGINEERING

pubs.acs.org/journal/abseba

Article

Microfibrous Extracellular Matrix Changes the Liver Hepatocyte Energy Metabolism via Integrins

Tianjiao Huang, Curtis G. Jones, Jay H. Chung, and Chengpeng Chen*

Cite This: *ACS Biomater. Sci. Eng.* 2020, 6, 5849−5856

Read Online

ACCESS | Metrics & More | Article Recommendations | Supporting Information

ABSTRACT: Cell line-based liver models are critical tools for liver-related studies. However, the conventional monolayer culture of hepatocytes, the most widely used *in vitro* model, does not have the extracellular matrix (ECM), which contributes to the three-dimensional (3D) arrangement of the hepatocytes in the liver. As a result, the metabolic properties of the hepatocytes in the monolayer tissue culture may not accurately reflect those of the hepatocytes in the liver. Here, we developed a modular platform for 3D hepatocyte cultures on fibrous ECMs produced by electrospinning, a technique that can turn a polymer solution to the micro/nanofibers and has been widely used to produce scaffolds for 3D cell cultures. Metabolomics quantitation by liquid chromatography−mass spectrometry (LC−MS) indicated that Huh7 hepatocytes grown in microfibers electrospun from silk fibroin exhibited reduced glycolysis and tricarboxylic acid (TCA) cycle, as compared to the cells cultured as a monolayer. Further mechanistic studies suggested that integrins were correlated to the ECM's effects. This is the first time to report how an ECM scaffold could affect the fundamental metabolism of the hepatocytes via integrins.

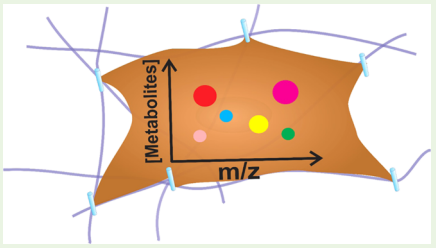

KEYWORDS: *electrospinning, silk fibroin, Huh7, fundamental metabolism, metabolomics, integrins*

INTRODUCTION

The liver carries out a number of essential functions, including blood detoxification, protein synthesis, regulation of energy balance, and production of other biochemicals to maintain the whole-body homeostasis.[1] In addition to these functions, the liver is also the main site of drug metabolism, making it vulnerable to drug toxicity; indeed, hepatotoxicity is one of the leading causes of drug failure.[2] Therefore, detecting the potential hepatotoxicity at the early stage of drug development/screening will minimize the failure rate and thus the cost of bringing a drug into the market. In this sense, hepatic models are invaluable tools in drug discovery and development.

There are two general families of hepatic models: *in vivo* and *in vitro*. The apparent advantage of the *in vivo* animal models (e.g., rodents) is the conservation of the organ- and system-level complexity.[3] However, animal models pose their own challenges. First, the throughput of the animal models is usually low because of the high time, labor, and monetary costs.[4] Also, the animal models typically test a single drug each time to avoid interferences, which further limits the throughput.[5] In addition, very high doses of compounds, sometimes orders of magnitude higher than those humans are exposed to, are required for animal experiments to generate clear results.[6]

The *in vitro* models, which utilize cell culture-based methodologies, can circumvent the throughput, cost, and dosing issues of the *in vivo* models.[6] For example, hepatocytes can be batch cultured in a multiwell plate treated with various drugs of different doses in one experiment. Three types of biocomponents are mainly used to fabricate an *in vitro* hepatic model: liver slices, primary hepatocytes, and hepatic cell lines. Despite the physiological relevance of liver tissue slices that retain liver structures and the cell types, the functions of the hepatocytes start decaying after 6 h of the tissue isolation.[7] Primary hepatocytes have similar enzyme activities as the physiological liver, but their functions decline fast during culture, and these cells are not available to every laboratory.[8] Immortalized hepatic cell lines such as Huh7 and HepG2 are long-lasting, retain liver-specific functions, and are easy to maintain.[9] Therefore, these cell lines have been widely used, especially for high-throughput initial drug screenings.[10] However, a significant number of findings from the cell line-based models cannot be reproduced in subsequent preclinical and clinical studies,[10] reflecting the inadequacies of the cell lines.[11]

For the hepatic cell lines to better simulate physiological functions, maintaining the relevant cell niche is critical. The standard protocol to culture cells as a two-dimensional (2D) monolayer in a container (e.g., flasks) cannot mimic the three-dimensional (3D) microenvironment of the cells in a liver,[12]

Received: September 3, 2020
Accepted: September 8, 2020
Published: September 17, 2020

https://dx.doi.org/10.1021/acsbiomaterials.0c01311
ACS Biomater. Sci. Eng. 2020, 6, 5849−5856

where the hepatocytes rest on and interact with 3D extracellular matrices (ECMs) containing fibrous microstructures, which can affect cell behaviors and functions.[13] Therefore, growing hepatic cell lines in a 3D ECM may better simulate the hepatocytes in the liver. With the advance of material science and microfabrication technologies, various *in vitro* 3D hepatic models have been reported.[14−16] Hepatocytes naturally aggregate to form spheroids in proper microcontainers;[17] thus, the microwell platforms were utilized for 3D hepatic spheroid culture. For example, Bhise et al. fabricated a microwell array using stamps on poly(dimethylsiloxane) (PDMS) with the successful spheroid formation of ∼200 μm diameter, which showed consistent production of albumin and responses to drugs.[18] Hydrogels, networks of polymer chains that are highly hydrated, were also applied as a 3D matrix for hepatic cell culture.[19−21] Precursors of the hydrogels premixed with the cells could be cured under physical (e.g., UV radiation) and chemical (e.g., cross-linker) conditions with desired shapes and dimensions via micromolds or bio-3D-printing.[22−24] Electrospinning, which uses a high voltage to turn a polymer solution to micro/nanofibers with tunable fiber and pore sizes,[25] is another technology used to fabricate the 3D fibrous ECMs. A myriad of cell types, including hepatocytes,[26] have been successfully 3D cultured on the electrospun fibers showing improved functions compared to the 2D monolayers.[27−30]

These approaches offer a great promise for the development of 3D liver models. However, previous studies limited their investigation to fingerprint the functions of the hepatocytes, including protein synthesis and secretion (mainly albumin),[18] CYP activities,[31] and responses to certain drugs/toxins.[11] While meaningful and informative, these did not investigate the impact of the ECMs on the critical metabolism features of hepatocytes, such as energy production. Fundamental metabolisms are the supporting poles of cell viability and functions, the disturbance of which can radically impair cellular activities.[32] Therefore, to create a 3D *in vitro* liver model, the impacts of scaffolding ECMs on the metabolism of the hepatic cell lines need to be understood. Here, we present our findings that microfibers electrospun from silk fibroin could modulate energy metabolism in the hepatic cell line Huh7. Further mechanistic investigation indicated that integrins were involved in the processes. This work is the first to report that ECMs play a role in hepatic basic metabolism, and the insight generated herein lays the groundwork for future hepatic modeling.

EXPERIMENTAL SECTION

Fabrication of the Silk Fibroin Fibers. The silk fibroin was extracted from silkworm cocoon following the well-established method by Rockwood et al.[33] Purified and lyophilized silk fibroin (from *Bombyx mori* silkworm) was dissolved in HFP (hexafluoroisopropanol; Millipore-Sigma, MO) at a concentration of 6% (w/v). The solution was loaded in a 3 mL syringe coupled with a 20-gauge blunt needle (2″ long). A syringe pump was used to deliver the fibroin solution at 1 mL/h. A voltage of 25 kV was applied to the syringe needle to generate the electrospun fibers at room temperature, which were deposited on a grounded stainless-steel plate (20 × 20 cm^2) placed 20 cm away from the needle. After 2 h of electrospinning, a layer of the silk fibroin fibers of ∼50 μm thick was collected.

Characterization of the Electrospun Fibers. We characterized the morphology of the fibrous scaffolds by a scanning electron microscope (SEM). After a sample was sputter-coated with gold (current = 20 mA; duration = 30 s), the sample was placed in the SEM chamber with a 15 kV electron beam to take images. A sample was imaged from both top and bottom sides to confirm the uniformity of the fibers. The software of ImageJ was utilized to measure the fiber diameter and the pore sizes as previously reported by others and us.[34,35] Briefly, to measure the fiber diameter, a straight line was drawn perpendicularly across a fiber in calibrated ImageJ. To measure the pore size, continuous segments of lines were drawn along a pore to form a closed polygon, the area of which was directly read out by ImageJ. On average, 50 random measurements were conducted on each image to determine the fiber diameter and pore sizes. A total of 10 samples were analyzed. The thickness of the fibrous layer was carefully measured on the SEM images of cross views (Figure S2 in the Supporting Information (SI)). The stiffness of the electrospun silk fibroin fibers was detected using an atomic force microscope (Veeco, NY) via a standard triangular silicon nitride cantilever with a nominal spring constant of 0.06 N/m and a tip radius within 20 nm.

Preparation of the Cell Culture Plate. The electrospun fibers were peeled off from the stainless-steel plate and spread on a polystyrene sheet (250 μm thick). Deionized water was sprayed on the fibers to further spread the fiber layer on the polystyrene sheet. After overnight drying, the two layers were bounded likely due to intermolecular forces. A laser cutter was then applied to cut discs of 34.5 mm out of the fiber−polystyrene sheet, which could fit precisely in a six-well plate. The cutting edges fused the fiber layer onto the polystyrene. Three discs with the fibers were placed in three wells of a six-well plate, while the remaining three wells contained discs of flat surfaces as controls for 2D monolayer culture. The flat discs were prepared by coating a layer of the silk fibroin solution on the polystyrene sheet as reported previously[36] to maintain identical surface chemistry with the fibrous scaffolds. All discs were sterilized by being soaked in 70% ethanol for 30 min, followed by air drying in UV.

Huh7 Cell Culture and Characterization. The Huh7 cells (ATCC, VA) with passage numbers between 2 and 5 were used. Dulbecco's modified Eagle's medium (DMEM) supplemented with 10% FBS and 1% pen−strep was applied for the cultures. A flask (T-75) of the cells at ∼90% confluency was trypsinized, centrifuged, and resuspended in fresh media at a density of 0.5 million cells/mL. Next, 2 mL of the cell suspension was added to each well containing either fibrous or flat substrates. This step was to seed the cells on the discs; after 2 h, 4 mL of the fresh media was added to each well. Media was changed every 24 h. The cells cultured for 48 h were used for subsequent studies.

The morphology of the cells was characterized on SEM images in the software of ImageJ. Specifically, on each image, 20 cells were randomly chosen and traced using the polygon tool of ImageJ. The area of the traced cells was then readout. The gaps between the adjacent cells were also measured using the straight line tool.

The proliferation was determined by measuring cell numbers on the scaffolds at different time points. The cell numbers were quantitated by detecting the amount of total proteins in the lysates. Specifically, after 12, 24, 36, and 48 h of the cell seeding, the substrates (fibrous and flat) were removed from the culture plate, followed by thorough rinsing with phosphate-buffered saline (PBS) and cell lysis in radioimmunoprecipitation assay (RIPA) buffer with an ultrasonic homogenizer (1 min). The protein concentrations in the lysates were assayed by the bicinchoninic acid (BCA) assay. Blanks were conducted by soaking the substrates (without cells) in the lysis buffer for the same duration, followed by BCA assaying. A calibration curve was obtained by lysing the known number of cells (0, 0.5, 1, 2, 4, and 8 million) and quantitating the proteins in the corresponding lysates.

The activity of cytochrome P450 (CYP450) of the hepatic cells was evaluated by 7-ethoxyresorufin. A stock solution of 7-ethoxyresorufin of 4.15 mM (1 mg/mL) was prepared in dimethyl sulfoxide (DMSO), which was then diluted in the cell culture media to a final concentration of 5.00 μM.[37] A total of 5 mL of this media was added to the wells with the hepatocytes that were cultured on fibers or on the flat. After 0, 2, 4, 6, 8, 10, 12, and 24 h, an aliquot of 50 μL (1% of the total volume) of the media was sampled, followed by adding 50 μL of fresh media (with 7-ethoxyresorufin) to maintain volumes

https://dx.doi.org/10.1021/acsbiomaterials.0c01311
ACS Biomater. Sci. Eng. 2020, 6, 5849−5856

unchanged. Fresh media containing 7-ethoxyresorufin was also measured as the blank. After 24 h, the cells on the insert in each well were thoroughly rinsed by PBS and then lysed. The amount of proteins in the lysates was measured by the BCA assay, as a measurement of the cell numbers in each well. The resorufin samples were then loaded in a 96-well plate for fluorescence measurements, the intensities of which were normalized to the cell numbers based on the BCA assay results.

The albumin secretion was measured by human albumin ELISA kits (Millipore-Sigma, MO). Urea secreted from the cells was quantitated by an enzyme-based colorimetric assay (Abcam, MA) following the user manual.

The viability of the cells was accessed via fluorescent live/dead imaging right before the intracellular metabolomics quantitation. The commercially available staining kit (ThermoFisher, PA) was used as instructed by the manufacturer. A fluorescent microscope (Zeiss, NJ) was utilized to take the images. Live cells were stained green, while dead cells being red.

Liquid Chromatography−Mass Spectrometry (LC−MS) Analyses of the Intracellular Metabolites of Interest. To take the cell lysates for intracellular metabolites quantitation, the media was aspirated in each well, followed by washing 3 times using PBS buffer (Millipore-Sigma, MO). After that, 400 μL of LCMS grade water at 0 °C (Millipore-Sigma, MO) was added to each well. An ultrasonic homogenizer probe was used to lyse the cells in each well for 1 min. An aliquot of 200 μL of the lysate was taken for the BCA protein assay, as a measurement of the cell numbers in each well for subsequent data normalization. The remaining lysates were mixed with 800 μL of acetonitrile/methanol (50/50; v/v) containing 10 μM ^{13}C-threonine (as the internal standard for the LC−MS analyses, purchased from Cambridge Isotope Laboratories, Inc., MA) and vortex-mixed for 30 s. Then, the samples were incubated for 1 h at −20 °C to precipitate proteins, which were then removed by being centrifuged at 14 000 rpm (Eppendorf, Centrifuge 5424R, NY) at 4 °C for 15 min. The supernatant was transferred to another clean vial, followed by lyophilizing (Savant from Thermo Scientific, MA). The dry extracts were reconstituted in 15 μL of LCMS grade water with 0.1% formic acid and transferred to LC−MS analyses.

LC−MS analyses were performed with an Agilent G6530C LC QTOF system equipped with the capillary HPLC 1260 Infinity series. For both positive and negative detection modes, a full scan range of 50 to 1000 m/z with a mass accuracy of 2 ppm was performed. For the positive mode, electrospray ionization (ESI) ion source parameters were gas temperature 320 °C, drying gas 10 L/min, nebulizer 30 psi, and capillary voltage 3500 V. The fragmentor, skimmer, and OCT1 RF Vpp were set to 110, 65, and 750 V, respectively. For the negative mode, ESI ion source parameters were gas temperature 300 °C, drying gas 10 L/min, nebulizer 30 psi, and capillary voltage 2700 V. The fragmentor, skimmer, and OCT1 RF Vpp were set to 90, 65, and 750 V, respectively.[38]

A C18 column (Luna Omega 1.6 μm, PS 100 Å with an inner diameter of 100 mm × 2.1 mm, Phenomenex, CA) was used with the following gradient: mobile phase A was 0.1% formic acid in water; mobile phase B was LC−MS grade methanol (Fisher Scientific, Hampton, NH). At positive mode, the gradient started with 100% A at 0 min and decreased to 0% A at 15 min. The A phase was remained at 0% till 25 min, followed by being increased to 100% at 30 min and held until 45 min. The flow rate was set at 30 μL/min. For negative mode, the gradient was the same but with a flow rate of 40 μL/min. An aliquot of 5 μL of the samples was injected into the column by an autosampler for each run.

The peak areas of the analytes of interest were analyzed by MassHunter Qualitative Analysis Version B.10, which were then normalized to the internal standard (^{13}C-threonine). The data were further normalized by the cell numbers in each culture well (by the BCA protein assay).

Immunoblotting. The cell lysates were harvested by adding 100 μL of RIPA buffer (radioimmunoprecipitation assay buffer with 150 mM sodium chloride, 1.0% NP-40, 0.5% sodium deoxycholate, 0.1% sodium dodecyl sulfate (SDS), and 50 mM Tris, pH 8.0) with complete protease inhibitor cocktail (Abcam, MA), being sonicated on ice on the day of analysis. The protein concentrations of the lysates were determined by the Coomassie protein assay kit following the manufacturer's manual (Thermo Scientific, MA). The cell lysates with 25 μg of total protein were subjected to 7% SDS-polyacrylamide gels (Bio-Rad, CA). After electrophoresis, the proteins were transferred into nitrocellulose membranes (Bio-Rad, CA). The membranes were blocked in PBST buffer (PBS with 0.1% Tween-20) containing 2% nonfat dry milk powder for 30 min at room temperature. Subsequently, the membranes were incubated overnight with rabbit-polyclonal anti-integrin β1 and rabbit-polyclonal anti-β-actin (1:1000) at 4 °C. After washing in PBST buffer, the membranes were incubated with horseradish peroxidase-conjugated antirabbit antibodies (1:1000). Immunoreactivity was detected using an Amersham Imager (GE Healthcare, MA). The band intensities were normalized to those of β-actin.

Integrin Inhibition. The peptide RGDS (arginine−glycine−aspartic acid−serine; R&D Systems, MN) was mixed in the media with the cells cultured on the flat surface for 48 h before the metabolomics studies. Estimated from the literature, 10, 50, and 100 μg/mL of the inhibitor were tested. It is known that intracellular cAMP is a downstream marker of integrin activities. Therefore, we measured the cAMP levels in the cells on the flat with the various inhibitor concentrations and compared them with that in the cells cultured on fibers, to determine the optimal inhibitor concentration. The peptide RGES (the third amino acid replaced by glutamic acid; GenScript USA Inc., NJ) was also applied as the negative control.

Statistics. All statistical analyses were performed using GraphPad Prism 7 and Microsoft Excel. The error bars were standard errors of mean (S.E.M.) unless otherwise stated. A significant difference was determined only when $p < 0.05$. For the metabolomics data in Figure 2, the percentage change of a metabolite was calculated by eq 1, where A_{3D} was the abundancy of the metabolite in the cells cultured on the 3D fibrous scaffold and A_{2D} was the abundancy in the cells on the flat stratum. The error bars were propagated S.E.M. One-sample t-test was applied to determine the significance of the percent changes with the standard value being 0% change. All other significant comparisons were conducted by the two-sample t-test.

$$\% \text{ change} = (A_{3D}/A_{2D} - 1) \times 100\% \quad (1)$$

RESULTS AND DISCUSSION

Human liver cell lines derived from hepatic carcinomas, including HepG2 and Huh7, have been widely applied in pharmaco-toxicology, drug screening, and physiological studies

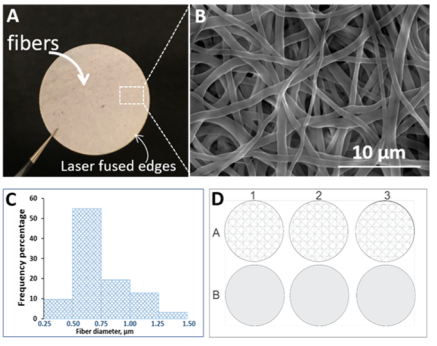

Figure 1. Research design. (A) Microfibers electrospun from silk fibroin were deposited on a polystyrene sheet, which was then laser cut to discs that can fit in a six-well plate. (B) SEM view of the electrospun fibers. The fiber diameter is 0.78 ± 0.37 μm (mean ± stdev). (C) Histogram shows the distribution of the fiber diameters. (D) Instead of culturing the cells directly on the bottom of the wells, circular inserts with desired ECMs (e.g., fibrous and flat) were used for cell cultures.

https://dx.doi.org/10.1021/acsbiomaterials.0c01311
ACS Biomater. Sci. Eng. 2020, 6, 5849−5856

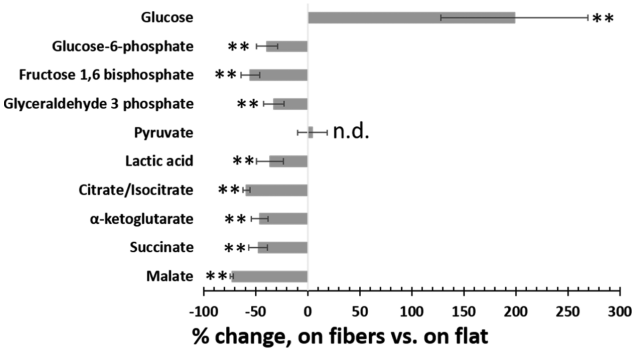

Figure 2. Energy metabolites in the Huh7 cells cultured on the fibers vs on the flat: three key metabolites in glycolysis and five key metabolites in the tricarboxylic acid (TCA) cycle were significantly decreased, indicating lower-energy metabolism. The glucose level was higher due to reduced glycolytic consumption. N = 15, error bar = S.E.M. $^{**}p < 0.01$, $^{*}p < 0.05$, n.d. = none significant difference.

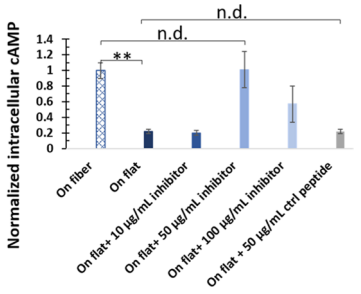

Figure 4. Efficacy of the integrin inhibitor RGDS. cAMP is a downstream marker of integrins—overexpression of integrins reduces intracellular cAMP. The cells cultured on the flat had significantly less cAMP than in the cells on the fibers, which was consistent with our integrin data. RGDS of 10 μg/mL could not efficiently inhibit integrins, as was reflected by the unchanged cAMP level. Both 50 and 100 μg/mL RGDS could increase cAMP, indicating integrin inhibition. However, the 50 μg/mL could restore the cAMP to the same level as in the cells on the fibers, which was thus determined as the optimal dose. We also tested a negative control peptide RGES, which could not block integrins (cAMP was not increased). N = 15, error bar = S.E.M. $^{**}p < 0.01$, n.d. = none significant difference.

due to availability.[39−41] However, significant differences exist between the cell lines and hepatocytes in the liver, making the *in vitro* results often irreproducible in subsequent trials.[42,43] To improve the predictivity and reproducibility of cell line-based assays, the discrepancies need to be minimized. Accumulating evidence suggests that the conventional way to culture the cells *in vitro* can be a cause of the discrepancies.[19,44] Cells grown in a 2D monolayer in a container or on a surface cannot recapitulate the *in vivo* microenvironment.[45] The cells *in vivo* are on 3D microfibrous ECMs, which can modulate cell behaviors and functions via two possible mechanisms:[46] (1) enhancing cell−cell interactions by defining the physical space between cells; (2) directly affecting the cellular pathways via ECM receptors such as integrins. A considerable volume of the literature has demonstrated the importance of 3D ECMs for *in vitro* hepatocyte cultures/studies[43]—"the third dimension bridges the gap between cell culture and the liver tissue".[47]

Electrospinning is a technique that can turn a polymer solution into micro/nanofibers as 3D cell culture scaffolds.[48] These scaffolds are highly fibrous and porous and thus can mimic physiological ECMs.[49] Compared to synthetic polymers (e.g., polystyrene), natural biopolymers are more preferred to electrospin scaffolds due to their chemical similarity to native ECMs.[50] Among the biopolymers, silk fibroin is an excellent material for cell cultures due to its unique advantages, including tunable mechanical strength, biocompatibility, non-toxicity, low immunogenicity, and relative ease in preparation.[51−53] These characteristics were recently insightfully reviewed with abundant details by Kundu et al.[54] Various cell types have been successfully cultured on silk fibroin scaffolds *in vitro* to enhance their physiological relevance.[36,52]

The liver is a key metabolic organ with active activities that can affect the liver itself and other organs/tissues.[55] The potential impacts of the ECM scaffolds on the hepatic fundamental metabolisms have not been investigated. Metabolomics, the study of the levels of the endogenous metabolites, which are the direct effector of the cellular machinery, allows for accessing cellular functions from a broad perspective.[32,56] Therefore, we studied the effects of the silk fibroin fibers on the fundamental metabolism of a widely used hepatic cell line, Huh7, with a focus on energy metabolism, which is a principle pole that supports the cell homeostasis.

ECM, Research Design, and Cell Cultures. Silk fibroin extracted from *Bombyx mori* silkworm was used to electrospin the fibrous scaffolds. Previous works by others and us suggested that the silk fibroin fibers with submicron diameters were an optimal scaffold for various cell types.[36,57,58] Therefore, we deduced that the scaffold was also suitable for

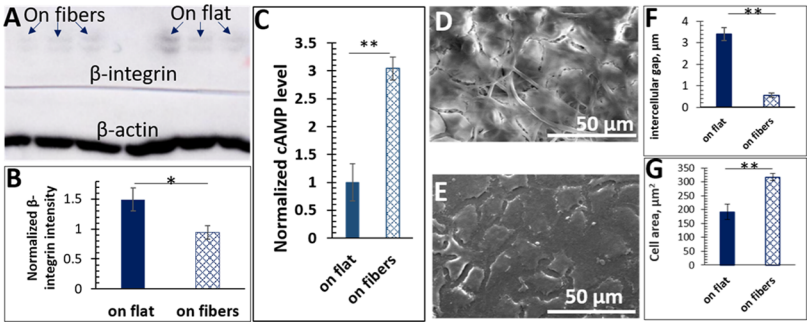

Figure 3. (A) Western blot results of β-integrin. The cells cultured on the flat stratum had more integrins. (B) Quantitation of the Western blot results (N = 7, error = S.E.M.). (C) Intracellular cAMP quantitation. It is known that integrin overexpression can reduce the cAMP levels. The data here (N = 15, error = S.E.M.) confirmed that integrins were overexpressed in the cells on the flat compared to those on the fibers. (D, E) Morphology of the cells cultured on the fibers vs on the flat. (F) Measured intercellular gaps for the cells on the fiber and on the flat (N = 50). (G) Measured cell areas on the fibers vs on the flat (N = 50, error = S.E.M.). For all of the panels: $^{*}p < 0.025$; $^{**}p < 0.01$.

https://dx.doi.org/10.1021/acsbiomaterials.0c01311
ACS Biomater. Sci. Eng. 2020, 6, 5849−5856

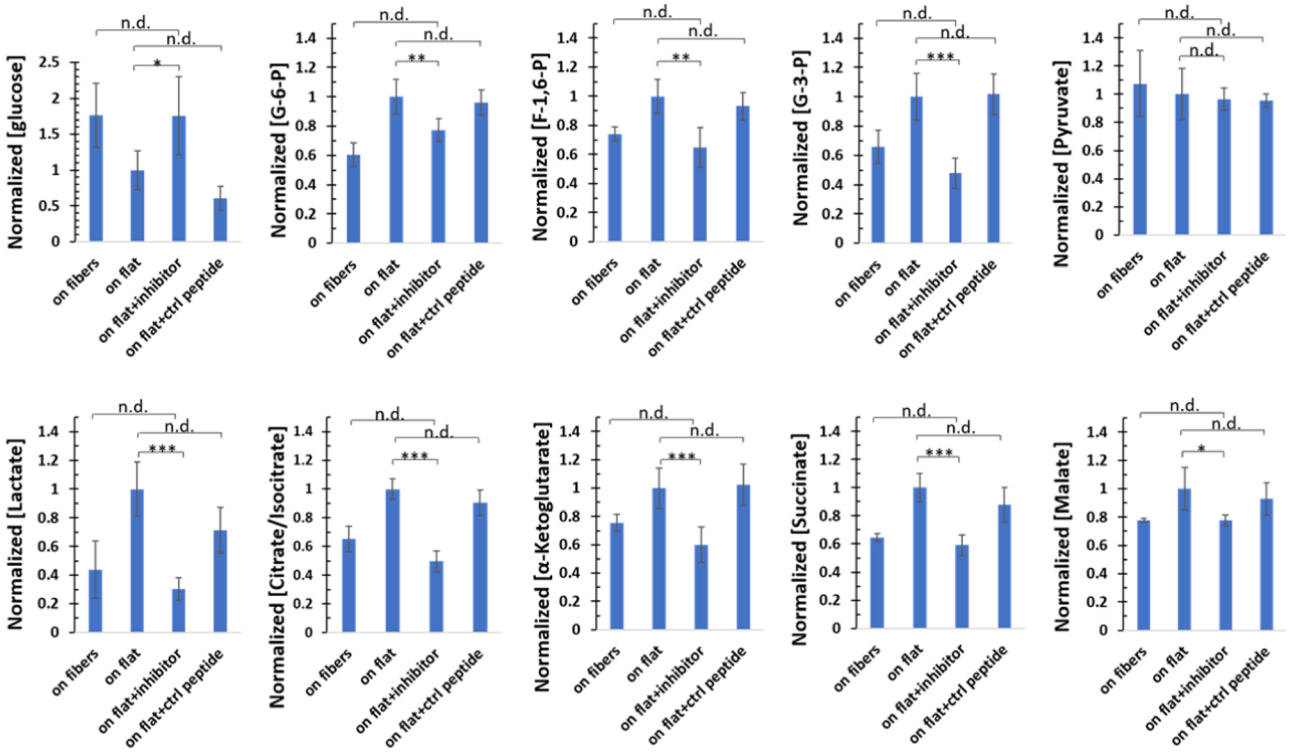

Figure 5. With the integrin inhibitor (50 μg/mL RGDS), all of the detected energy metabolites were restored to the same level as in the cells on the fibers. As a control, the RGES (ctrl peptide; 50 μg/mL) could not exert the effects. N = 15, error bars = S.E.M., *p < 0.05, **p < 0.025, ***p < 0.01, n.d. = none significant difference. G-6-P = glucose-6-phosphate; F-1,6-P = fructose-1,6-phosphate; G-3-P = glyceraldehyde-3-phosphate.

the hepatocytes. The fibers were placed on a polystyrene sheet, which was then laser cut to discs (Figure 1A) that fit in a multiwell plate. The laser cutting also fused the edges of the fibers and the polystyrene to permanently bond the two layers. The polystyrene acted as a support structure so that the flimsy fibers would not be compromised when adding or removing media. Specifically, we utilized a six-well plate to ensure sufficient cell numbers for the subsequent metabolomics measurements (Figure 1D). Other plate formats such as a 96-well plate can also be used (Figure S1 in the SI).

The electrospun fibers were characterized via standard protocols. A SEM image of the fibrous scaffolds is shown in Figure 1B and the average diameter of the fibers was calculated by ImageJ as 0.78 ± 0.37 μm (n = 500, mean ± stdev), with most fibers distributed in the 0.50−1.00 μm range (Figure 1C). The average pore size of the scaffolds was 61 ± 13 μm^2. The fiber and pore sizes between the batches were consistent with variances of <5%. As ECM stiffness can affect cellular behaviors and functions,[59] we also assessed the silk fibroin fibers using an atomic force microscope (AFM). The average stiffness was found to be 3.2 ± 0.8 kPa, which was within the physiological range of liver stiffness (2.3−5.9 kPa).[60] Figure S2 in the SI demonstrated a SEM cross-view of the fiber layer thickness, which was 50 ± 3 μm.

We then conducted fundamental characterizations of the Huh7 cells cultured on the fibers and on the flat surface, including proliferation, viability, CYP activity, albumin synthesis, and urea production. As shown in Figure S3A,B in the SI, cellular proliferation increased over time, with the final coverage being around 90% after 48 h. The cell coverage was similar between the cells on the fibers vs on the flat at each time point (every 12 h; Figure S3C in the SI). Cell viability, which was evaluated by live/dead (green/red) fluorescent staining, was also similar after 48 h (Figure S3D,E). We quantitated the cell numbers by assaying total protein content every 12 h and found that after 48 h, there were ∼25% (N = 10, p < 0.05) more cells on the fibers than on the flat surface (Figure S4A). This difference was likely caused by the infiltration of the cells into the pores of the fibrous scaffold, which is visible in the confocal image in Figure S4B.

The activity of CYP450, important hepatocyte enzymes, was evaluated using 7-ethoxyresorufin, a commonly used fluorescent substrate of CYP450.[37] After being hydrolyzed by CYP1A1, CYP1A2, and/or CYP1B1, resorufin is produced with bright fluorescence emission at 585 nm. As can be seen in Figure S5A in the SI, the CYP activities increased as a function of time on both surfaces, but they were higher in the cells cultured on fibrous inserts. We also found that the cells on the fibrous scaffold synthesized slightly more albumin and urea (Figures S5B,C).

Effects of the Fibrous ECM on the Energy Metabolism in the Huh7 Cells. Among the numerous metabolic routes, energy metabolism encompasses critical bioprocesses such as intracellular oxidative phosphorylation, bioenergetic, biosynthetic, and redox homeostasis.[61,62] For instance, elevated glycolysis can perturb de novo synthesis of fatty acid and the production of ribose 5-phosphate for nucleotide synthesis.[63] Therefore, to understand the roles of scaffolding materials in cell biology, it is critically necessary to first evaluate if and how the ECM can impact the energy metabolism—glycolysis and TCA cycle (tricarboxylic acid cycle).

We therefore lysed the cells cultured on the fibrous scaffold and on the flat surface and measured the intracellular metabolites in the glycolysis and TCA pathways using the targeted liquid chromatography−mass spectrometry (LC−MS) methodology. Targeted analyses offer specific measure-

https://dx.doi.org/10.1021/acsbiomaterials.0c01311
ACS Biomater. Sci. Eng. 2020, 6, 5849−5856

ments of the specific pathways with the well-characterized metabolites of each pathway. We targeted all intermediate metabolites in glycolysis including glucose, glucose-6-phosphate, fructose-6-phosphate, fructose-1,6-biphosphate, dihydroxyacetone phosphate, glyceraldehyde-3-phosphate, 1,3-bisglyceralphosphate, 3-phosphoglycerate, 2-phosphoglycerate, phosphoenolpyruvate, and pyruvate and in the TCA cycle including citrate, cis-aconitate, D-isocitrate, α-ketoglutarate, succinate-coA, succinate, fumarate, malate, and oxaloacetate. Due to technical challenges,[56] certain molecules did not show quantitative signals in the complex samples such as cell lysates in LC−MS. Therefore, we reported here only metabolites with signal-to-noise (S/N) ratios higher than 10.

As shown in Figure 2, glucose-6-phosphate, fructose-6-phosphate, and glyceraldehyde-3-phosphate, the three key metabolites in glycolysis, were significantly decreased in the cells on the fibrous scaffold, indicating reduced glycolysis. Meanwhile, we found that the abundances of the five major metabolites in the TCA cycle, citrate/isocitrate, succinate, α-ketoglutarate, and malate, were also significantly reduced. Perhaps due to the decreased glucose metabolism (glycolysis and TCA cycle), the glucose level in the cells cultured on the fibers was higher. These data suggest that the silk fibroin fibers could decrease energy metabolism in the Huh7 cells.

Mechanistic Exploration. These findings prompted us to investigate how the fibrous ECM modulated metabolism and, in particular, the identity of the membrane receptor that mediated the ECM effect. Integrins, which are composed of α and β subunits,[64] are the transmembrane receptors for ECMs. Integrins are mostly expressed at the cell−ECM contact regions (focal adhesion),[65] and the microstructure of an ECM determines focal adhesion.[66] Most cell types *in vivo* are embedded in 3D fibrous ECMs via pseudopodia structures with integrins concentrated at the cell−ECM contacting spots.[67] However, with a 2D flattened ECM, a cell contacts the ECM stratum with a whole side of the cellular body, which will likely cause integrin overexpression. Delcommenne et al. found that the primary epithelial cells express drastically more integrins when cultured on a tissue plate than on the native fibrous basement membrane.[68] These findings suggest that the fibrous scaffold may decrease integrin expression in the Huh7 cells and thus affect energy metabolism.

We began to study the potential role of integrins in the metabolic effects of the ECM by measuring the levels of β integrins via Western blot. As shown in Figure 3A,B, the cells on the flat had significantly more integrins ($p < 0.025$). It is known that a higher integrin level can decrease intracellular cAMP via the β-adrenergic receptor (β-AR)[69−71] and the G_α protein,[72] and that integrin overexpression can increase actin polymerization,[73] which causes the cells to contract and thereby enlarge intercellular gaps. Consistent with this, the cells on the fibers indeed had higher cAMP content (Figure 3C) and larger area and smaller intercellular gaps (Figure 3D−G). These data further supported our observation that the ECM fibers decreased integrins in the cells.

To investigate the integrin overexpression in the cells on the flat contributed to the metabolism changes, we blocked the integrins in the cells cultured on the flat surface with the known integrin inhibiting peptide RGDS (arginine−glycine−aspartic acid−serine).[74] We first measured the intracellular cAMP levels in the presence of varying concentrations of RGDS. As shown in Figure 4, 50 μg/mL RGDS and 100 μg/mL could both significantly increase cAMP, but the 50 μg/mL dose increased the cAMP levels in the cells cultured on the flat to that of the cells on the fibers, whereas a control peptide RGES, with the third amino acid (D/aspartic acid) replaced by E (glutamic acid), did not change the cAMP levels. Consistent with this, 50 μg/mL RGDS restored all of the detected metabolites in glycolysis and TCA cycle in the cells on the flat to that of those cultured on the fibrous ECM (Figure 5). In contrast, the RGES peptide (flat + ctrl peptide) did not affect the levels of these metabolites. Taken together, these findings indicate that the fibrous ECM decreased integrin expression and the metabolites of the glycolytic pathway and the TCA cycle in the Huh7 cells compared to the 2D flat cultures.

CONCLUSIONS

Our work showed that a fibrous scaffold made from silk fibroin reduced energy metabolism in Huh7 hepatocytes. This is the first study to report the effects of an ECM on the basic metabolism of the hepatocytes cultured *in vitro*. Further mechanistic studies indicated that the ECM tuned energy metabolism via the integrins. Overall, this work enhances our understanding of the roles of ECM in cellular biology.

ASSOCIATED CONTENT

Supporting Information

The Supporting Information is available free of charge at https://pubs.acs.org/doi/10.1021/acsbiomaterials.0c01311.

Other multiwell plate format with the ECM discs; SEM view of the fibers on the PS support structure; characterization of cell proliferation; measurements of CYP450 activity, albumin production, and urea synthese (PDF)

AUTHOR INFORMATION

Corresponding Author

Chengpeng Chen − *The Department of Chemistry and Biochemistry, University of Maryland, Baltimore County, Baltimore, Maryland 21250, United States;* orcid.org/0000-0001-7754-344X; Phone: +1-4104553053; Email: cpchen@umbc.edu

Authors

Tianjiao Huang − *Laboratory of Obesity and Aging Research, Cardiovascular Branch, National Heart Lung and Blood Institute, National Institutes of Health, Bethesda, Maryland 20892, United States*

Curtis G. Jones − *The Department of Chemistry and Biochemistry, University of Maryland, Baltimore County, Baltimore, Maryland 21250, United States*

Jay H. Chung − *Laboratory of Obesity and Aging Research, Cardiovascular Branch, National Heart Lung and Blood Institute, National Institutes of Health, Bethesda, Maryland 20892, United States*

Complete contact information is available at: https://pubs.acs.org/10.1021/acsbiomaterials.0c01311

Notes

The authors declare no competing financial interest.

ACKNOWLEDGMENTS

This work was supported by the startup funding of UMBC and the Intramural Research Program of National Heart Lung and Blood Institute, National Institutes of Health. We thank the

NHLBI Biochemistry Core and Dr. Duck-Yeon Lee's assistance for Mass Spectrometry and the Keith Porter Imaging Center at UMBC.

REFERENCES

(1) Fausto, N.; Campbell, J. S.; Riehle, K. J. Liver regeneration. *Hepatology* **2006**, *43*, S45−S53.
(2) Kaplowitz, N. Idiosyncratic drug hepatotoxicity. *Nat. Rev. Drug Discovery* **2005**, *4*, 489−499.
(3) Haugabook, S. J.; Ferrer, M.; Ottinger, E. A. In vitro and in vivo translational models for rare liver diseases. *Biochim. Biophys. Acta, Mol. Basis Dis.* **2019**, *1865*, 1003−1018.
(4) Vinken, M. Liver-based in vitro models for toxicity testing. *Toxicol. Lett.* **2018**, *295*, S7.
(5) Orbach, S. M.; Less, R. R.; Kothari, A.; Rajagopalan, P. In Vitro Intestinal and Liver Models for Toxicity Testing. *ACS Biomater. Sci. Eng.* **2017**, *3*, 1898−1910.
(6) Soldatow, V. Y.; LeCluyse, E. L.; Griffith, L. G.; Rusyn, I. In vitro models for liver toxicity testing. *Toxicol. Res.* **2013**, *2*, 23−39.
(7) Lake, B. G.; Beamand, J. A.; Wield, P. T.; Price, R. J. Use of precision-cut liver slices to evaluate species differences in 2-acetylaminofluorene-induced unscheduled DNA synthesis. *Toxicol. Appl. Pharmacol.* **1996**, *138*, 231−241.
(8) Lauschke, V. M.; Shafagh, R. Z.; Hendriks, D. F. G.; Ingelman-Sundberg, M. 3D Primary Hepatocyte Culture Systems for Analyses of Liver Diseases, Drug Metabolism, and Toxicity: Emerging Culture Paradigms and Applications. *Biotechnol. J.* **2019**, *14*, No. 1800347.
(9) Ramboer, E.; Vanhaecke, T.; Rogiers, V.; Vinken, M. Immortalized Human Hepatic Cell Lines for In Vitro Testing and Research Purposes. In *Methods in Molecular Biology*; Humana Press: New York, NY, 2015; Vol. *1250*, pp 53−76.
(10) Pati, F.; Gantelius, J.; Svahn, H. A. 3D Bioprinting of Tissue/Organ Models. *Angew. Chem., Int. Ed.* **2016**, *55*, 4650−4665.
(11) Poloznikov, A.; Gazaryan, I.; Shkurnikov, M.; Nikulin, S.; Drapkina, O.; Baranova, A.; Tonevitsky, A. In Vitro and In Silico Liver Models: Current Trends, Challenges and Opportunities. *ALTEX* **2018**, *35*, 397−412.
(12) Lei, K. F.; Chang, C. H.; Chen, M. J. Paper/PMMA Hybrid 3D Cell Culture Microfluidic Platform for the Study of Cellular Crosstalk. *ACS Appl. Mater. Interfaces* **2017**, *9*, 13092−13101.
(13) Chen, Z. W.; Zhao, R. G. Engineered Tissue Development in Biofabricated 3D Geometrical Confinement-A Review. *ACS Biomater. Sci. Eng.* **2019**, *5*, 3688−3702.
(14) Petropolis, D. B.; Faust, D. M.; Tolle, M.; Riviere, L.; Valentin, T.; Neuveut, C.; Hernandez-Cuevas, N.; Dufour, A.; Olivo-Marin, J. C.; Guillen, N. Human Liver Infection in a Dish: Easy-To-Build 3D Liver Models for Studying Microbial Infection,. *PLoS One* **2016**, *11*, No. e0148667.
(15) No, D. Y.; Lee, K. H.; Lee, J.; Lee, S. H. 3D liver models on a microplatform: well-defined culture, engineering of liver tissue and liver-on-a-chip. *Lab Chip* **2015**, *15*, 3822−3837.
(16) Prodanov, L.; Jindal, R.; Bale, S. S.; Hegde, M.; McCarty, W. J.; Golberg, I.; Bhushan, A.; Yarmush, M. L.; Usta, O. B. Long-term maintenance of a microfluidic 3D human liver sinusoid. *Biotechnol. Bioeng.* **2016**, *113*, 241−246.
(17) Takayama, K.; Kawabata, K.; Nagamoto, Y.; Kishimoto, K.; Tashiro, K.; Sakurai, F.; Tachibana, M.; Kanda, K.; Hayakawa, T.; Furue, M. K.; Mizuguchi, H. 3D spheroid culture of hESC/hiPSC-derived hepatocyte-like cells for drug toxicity testing. *Biomaterials* **2013**, *34*, 1781−1789.
(18) Bhise, N. S.; Manoharan, V.; Massa, S.; Tamayol, A.; Ghaderi, M.; Miscuglio, M.; Lang, Q.; Zhang, Y. S.; Shin, S. R.; Calzone, G.; Annabi, N.; Shupe, T. D.; Bishop, C. E.; Atala, A.; Dokmeci, M. R.; Khademhosseini, A. A liver-on-a-chip platform with bioprinted hepatic spheroids. *Biofabrication* **2016**, *8*, No. 014101.
(19) Guo, J. L.; Kim, Y. S.; Mikos, A. G. Biomacromolecules for Tissue Engineering: Emerging Biomimetic Strategies. *Biomacromolecules* **2019**, *20*, 2904−2912.
(20) Prince, E.; Alizadehgiashi, M.; Campbell, M.; Khuu, N.; Albulescu, A.; De France, K.; Ratkov, D.; Li, Y. F.; Hoare, T.; Kumacheva, E. Patterning of Structurally Anisotropic Composite Hydrogel Sheets. *Biomacromolecules* **2018**, *19*, 1276−1284.
(21) Terrell, J. A.; Jones, C. G.; Kabandana, G. K. M.; Chen, C. From cells-on-a-chip to organs-on-a-chip: scaffolding materials for 3D cell culture in microfluidics. *J. Mater. Chem. B* **2020**, *8*, 6667−6685.
(22) Ouyang, L. L.; Highley, C. B.; Rodell, C. B.; Sun, W.; Burdick, J. A. 3D Printing of Shear-Thinning Hyaluronic Acid Hydrogels with Secondary Cross-Linking. *ACS Biomater. Sci. Eng.* **2016**, *2*, 1743−1751.
(23) Patel, N. R.; Whitehead, A. K.; Newman, J. J.; Caldorera-Moore, M. E. Poly(ethylene glycol) Hydrogels with Tailorable Surface and Mechanical Properties for Tissue Engineering Applications. *ACS Biomater. Sci. Eng.* **2017**, *3*, 1494−1498.
(24) Xue, J. J.; Wu, T.; Dai, Y. Q.; Xia, Y. N. Electrospinning and Electrospun Nanofibers: Methods, Materials, and Applications. *Chem. Rev.* **2019**, *119*, 5298−5415.
(25) Gholipourmalekabadi, M.; Khosravimelal, S.; Nokhbedehghan, Z.; Sameni, M.; Jajarmi, V.; Urbanska, A. M.; Mirzaei, H.; Salimi, M.; Chauhan, N. P. S.; Mobaraki, M.; Reis, R. L.; Samadikuchaksaraei, A.; Kundu, S. C. Modulation of Hypertrophic Scar Formation Using Amniotic Membrane/Electrospun Silk Fibroin Bilayer Membrane in a Rabbit Ear Model. *ACS Biomater. Sci. Eng.* **2019**, *5*, 1487−1496.
(26) Brown, J. H.; Das, P.; DiVito, M. D.; Ivancic, D.; Tan, L. P.; Wertheim, J. A. Nanofibrous PLGA electrospun scaffolds modified with type I collagen influence hepatocyte function and support viability in vitro. *Acta Biomater.* **2018**, *73*, 217−227.
(27) Chan, E. W. C.; Bennet, D.; Baek, P.; Barker, D.; Kim, S.; Travas-Sejdic, J. Electrospun Polythiophene Phenylenes for Tissue Engineering. *Biomacromolecules* **2018**, *19*, 1456−1468.
(28) Kang, Y.; Wang, C. L.; Qiao, Y. B.; Gu, J. W.; Zhang, H.; Peijs, T.; Kong, J.; Zhang, G. C.; Shi, X. T. Tissue-Engineered Trachea Consisting of Electrospun Patterned scPLA/GO-g-IL Fibrous Membranes with Antibacterial Property and 3D-Printed Skeletons with Elasticity. *Biomacromolecules* **2019**, *20*, 1765−1776.
(29) Jin, S.; Sun, F. H.; Zou, Q.; Huang, J. H.; Zuo, Y.; Li, Y. B.; Wang, S. P.; Cheng, L.; Man, Y.; Yang, F.; Li, J. D. Fish Collagen and Hydroxyapatite Reinforced Poly(lactide-co-glycolide) Fibrous Membrane for Guided Bone Regeneration. *Biomacromolecules* **2019**, *20*, 2058−2067.
(30) Li, N.; Xue, F. X.; Zhang, H.; Sanyour, H. J.; Ricke, A. P.; Uttecht, A.; Fanta, B.; Hu, J. L.; Hong, Z. K. Fabrication and Characterization of Pectin Hydrogel Nanofiber Scaffolds for Differentiation of Mesenchymal Stem Cells into Vascular Cells. *ACS Biomater. Sci. Eng.* **2019**, *5*, 6511−6519.
(31) Mandon, M.; Huet, S.; Dubreil, E.; Fessard, V.; Le Hegarat, L. Three-dimensional HepaRG spheroids as a liver model to study human genotoxicity in vitro with the single cell gel electrophoresis assay. *Sci. Rep.* **2019**, *9*, No. 10548.
(32) Huang, T.; Armbruster, M.; Lee, R.; Hui, D. S.; Edwards, J. L. Metabolomic analysis of mammalian cells and human tissue through one-pot two stage derivatizations using sheathless capillary electrophoresis-electrospray ionization-mass spectrometry. *J. Chromatogr. A* **2018**, *1567*, 219−225.
(33) Rockwood, D. N.; Preda, R. C.; Yucel, T.; Wang, X. Q.; Lovett, M. L.; Kaplan, D. L. Materials fabrication from Bombyx mori silk fibroin. *Nat. Protoc.* **2011**, *6*, 1612−1631.
(34) Sill, T. J.; von Recum, H. A. Electrospinning: applications in drug delivery and tissue engineering. *Biomaterials* **2008**, *29*, 1989−2006.
(35) Chen, C.; Mehl, B. T.; Sell, S. A.; Martin, R. S. Use of electrospinning and dynamic air focusing to create three-dimensional cell culture scaffolds in microfluidic devices. *Analyst* **2016**, *141*, 5311−5320.
(36) Chen, C. P.; Townsend, A. D.; Hayter, E. A.; Birk, H. M.; Sell, S. A.; Martin, R. S. Insert-based microfluidics for 3D cell culture with analysis. *Anal. Bioanal. Chem.* **2018**, *410*, 3025−3035.

https://dx.doi.org/10.1021/acsbiomaterials.0c01311
ACS Biomater. Sci. Eng. 2020, 6, 5849−5856

(37) Ghosal, A.; Hapangama, N.; Yuan, Y.; Lu, X. W.; Horne, D.; Patrick, J. E.; Zbaida, S. Rapid determination of enzyme activities of recombinant human cytochromes P450, human liver microsomes and hepatocytes. *Biopharm. Drug Dispos.* **2003**, *24*, 375−384.
(38) Huang, T.; Rabus, J. M.; Bythell, B. J.; Edwards, J. L. Fragmentation of Multi-charged Derivatized Lysine Using Nanospray CID Tandem Mass Spectrometry. *J. Am. Soc. Mass Spectrom.* **2019**, *30*, 1158−1162.
(39) Gutiérrez-García, A. K.; Choudhury, M.; De Leon-Rodriguez, A. Diisononyl Phthalate Differentially Affects Sirtuin Expression in the HepG2 Cell Line. *Chem. Res. Toxicol.* **2019**, *32*, 1863−1870.
(40) Tamam, H.; Park, J.; Gadalla, H. H.; Masters, A. R.; Abdel-Aleem, J. A.; Abdelrahman, S. I.; Abdelrahman, A. A.; Lyle, L. T.; Yeo, Y. Development of Liposomal Gemcitabine with High Drug Loading Capacity. *Mol. Pharmaceutics* **2019**, *16*, 2858−2871.
(41) Harupa, A.; De Las Heras, L.; Colmenarejo, G.; Lyons-Abbott, S.; Reers, A.; Caballero Hernandez, I.; Chung, C. W.; Charter, D.; Myler, P. J.; Fernandez-Menendez, R. M.; Calderon, F.; Palomo, S.; Rodriguez, B.; Berlanga, M.; Herreros-Aviles, E.; Staker, B. L.; Fernandez Alvaro, E.; Kaushansky, A. Identification of Selective Inhibitors of Plasmodium N-Myristoyltransferase by High-Throughput Screening. *J. Med. Chem.* **2020**, *63*, 591−600.
(42) Rezaee, R.; Abdollahi, M. The importance of translatability in drug discovery. *Expert Opin. Drug Discovery* **2017**, *12*, 237−239.
(43) Agarwal, T.; Subramanian, B.; Maiti, T. K. Liver Tissue Engineering: Challenges and Opportunities. *ACS Biomater. Sci. Eng.* **2019**, *5*, 4167−4182.
(44) Breslin, S.; O'Driscoll, L. Three-dimensional cell culture: the missing link in drug discovery. *Drug Discovery Today* **2013**, *18*, 240−249.
(45) Evans, V. J.; Hawkins, N. M.; Westfall, B. B.; Earle, W. R. Studies on Culture Lines Derived from Mouse Liver Parenchymatous Cells Grown in Long-Term Tissue Culture. *Cancer Res.* **1958**, *18*, 261−266.
(46) Hay, E. D. Collagen and other matrix glycoproteins in embryogenesis. In *Cell Biology of Extracellular Matrix*, 2nd ed.; Springer: Boston, MA, 1991.
(47) Pampaloni, F.; Reynaud, E. G.; Stelzer, E. H. K. The third dimension bridges the gap between cell culture and live tissue. *Nat. Rev. Mol. Cell Biol.* **2007**, *8*, 839−845.
(48) Bhardwaj, N.; Kundu, S. C. Electrospinning: a fascinating fiber fabrication technique. *Biotechnol. Adv.* **2010**, *28*, 325−347.
(49) Kishan, A. P.; Cosgriff-Hernandez, E. M. Recent advancements in electrospinning design for tissue engineering applications: A review. *J. Biomed. Mater. Res., Part A* **2017**, *105*, 2892−2905.
(50) Soares, R. M. D.; Siqueira, N. M.; Prabhakaram, M. P.; Ramakrishna, S. Electrospinning and electrospray of bio-based and natural polymers for biomaterials development. *Mater. Sci. Eng., C* **2018**, *92*, 969−982.
(51) Kundu, S. C.; Kundu, B.; Talukdar, S.; Bano, S.; Nayak, S.; Kundu, J.; Mandal, B. B.; Bhardwaj, N.; Botlagunta, M.; Dash, B. C.; Acharya, C.; Ghosh, A. K. Invited review nonmulberry silk biopolymers. *Biopolymers* **2012**, *97*, 455−467.
(52) Patra, C.; Talukdar, S.; Novoyatleva, T.; Velagala, S. R.; Muhlfeld, C.; Kundu, B.; Kundu, S. C.; Engel, F. B. Silk protein fibroin from *Antheraea mylitta* for cardiac tissue engineering. *Biomaterials* **2012**, *33*, 2673−2680.
(53) Farokhi, M.; Mottaghitalab, F.; Fatahi, Y.; Khademhosseini, A.; Kaplan, D. L. Overview of Silk Fibroin Use in Wound Dressings. *Trends Biotechnol.* **2018**, *36*, 907−922.
(54) Kundu, B.; Rajkhowa, R.; Kundu, S. C.; Wang, X. Silk fibroin biomaterials for tissue regenerations. *Adv. Drug Delivery Rev.* **2013**, *65*, 457−470.
(55) Mitra, V.; Metcalf, J. Metabolic functions of the liver. *Anaesth. Intensive Care Med.* **2012**, *13*, 54−55.
(56) Huang, T.; Armbruster, M. R.; Coulton, J. B.; Edwards, J. L. Chemical Tagging in Mass Spectrometry for Systems Biology. *Anal. Chem.* **2019**, *91*, 109−125.
(57) Chen, C.; Townsend, A. D.; Sell, S. A.; Martin, R. S. Microchip-based 3D-Cell Culture Using Polymer Nanofibers Generated by Solution Blow Spinning. *Anal. Methods* **2017**, *9*, 3274−3283.
(58) Munshi, A. S.; Chen, C. P.; Townsend, A. D.; Martin, R. S. Use of 3D printing and modular microfluidics to integrate cell culture, injections and electrochemical analysis. *Anal. Methods* **2018**, *10*, 3364−3374.
(59) Kumar, S. Stiffness does matter. *Nat. Mater.* **2014**, *13*, 918−920.
(60) Sporea, I.; Sirli, R.; Deleanu, A.; Popescu, A.; Cornianu, M. Liver stiffness measurement by transient elastography in clinical practice. *J. Gastrointestin Liver Dis.* **2008**, *17*, 395−399.
(61) Rui, L. Energy Metabolism in the Liver. *Compr. Physiol.* **2011**, *4*, 177−197.
(62) Huang, T.; Toro, M.; Lee, R.; Hui, D. S.; Edwards, J. L. Multi-functional derivatization of amine, hydroxyl, and carboxylate groups for metabolomic investigations of human tissue by electrospray ionization mass spectrometry. *Analyst* **2018**, *143*, 3408−3414.
(63) Adeva-Andany, M. M.; Perez-Felpete, N.; Fernandez-Fernandez, C.; Donapetry-Garcia, C.; Pazos-Garcia, C. Liver glucose metabolism in humans. *Biosci. Rep.* **2016**, *36*, No. e00416.
(64) Takada, Y.; Ye, X. J.; Simon, S. The integrins. *Genome Biol.* **2007**, *8*, 215.
(65) Uttayarat, P.; Toworfe, G. K.; Dietrich, F.; Lelkes, P. I.; Composto, R. J. Topographic guidance of endothelial cells on silicone surfaces with micro- to nanogrooves: Orientation of actin filaments and focal adhesions. *J. Biomed. Mater. Res., Part A* **2005**, *75a*, 668−680.
(66) Kim, H. N.; Kim, J. Effect of Topographical Feature Size on the Trend of Cell Behaviors. *IEEE Trans. Nanotechnol.* **2018**, *17*, 377−380.
(67) Kanchanawong, P.; Shtengel, G.; Pasapera, A. M.; Ramko, E. B.; Davidson, M. W.; Hess, H. F.; Waterman, C. M. Nanoscale architecture of integrin-based cell adhesions. *Nature* **2010**, *468*, 580−584.
(68) Delcommenne, M.; Streuli, C. H. Control of Integrin Expression by Extracellular-Matrix. *J. Biol. Chem.* **1995**, *270*, 26794−26801.
(69) Cheng, Q.; Ross, R. S.; Walsh, K. B. Overexpression of the integrin beta(1A) subunit and the beta(1A) cytoplasmic domain modifies the beta-adrenergic regulation of the cardiac L-type Ca(2+)current. *J. Mol. Cell. Cardiol.* **2004**, *36*, 809−19.
(70) Teoh, C. M.; Tam, J. K.; Tran, T. Integrin and GPCR Crosstalk in the Regulation of ASM Contraction Signaling in Asthma. *J. Allergy* **2012**, *2012*, No. 341282.
(71) Meyer, C. J.; Alenghat, F. J.; Rim, P.; Fong, J. H. J.; Fabry, B.; Ingber, D. E. Mechanical control of cyclic AMP signalling and gene transcription through integrins. *Nat. Cell Biol.* **2000**, *2*, 666−668.
(72) Alenghat, F. J.; Tytell, J. D.; Thodeti, C. K.; Derrien, A.; Ingber, D. F. Mechanical Control of cAMP Signaling Through Integrins Is Mediated by the Heterotrimeric G alpha s Protein. *J. Cell. Biochem.* **2009**, *106*, 529−538.
(73) DeMali, K. A.; Wennerberg, K.; Burridge, K. Integrin signaling to the actin cytoskeleton. *Curr. Opin. Cell Biol.* **2003**, *15*, 572−582.
(74) Keasey, M. P.; Jia, C. H.; Pimentel, L. F.; Sante, R. R.; Lovins, C.; Hagg, T. Blood vitronectin is a major activator of LIF and IL-6 in the brain through integrin-FAK and uPAR signaling. *J. Cell Sci.* **2018**, *131*, No. jcs202580.

https://dx.doi.org/10.1021/acsbiomaterials.0c01311
ACS Biomater. Sci. Eng. 2020, 6, 5849−5856